Influence of large signal modulation on photonic UWB generation based on electro-optic modulator

Rong Gu,[1,2] Shilong Pan,[1,*] Xiangfei Chen,[2] Minghai Pan[1] and De Ben[1]

[1]*College of Electronic and Information Engineering, Nanjing University of Aeronautics and Astronautics, Nanjing, 210016, China*

[2]*Nanjing National Laboratory of Microstructures and School of Engineering and Applied Sciences, Nanjing University, Nanjing 210093, China*

**pans@nuaa.edu.cn*

Abstract: Various schemes based on electro-optic modulators have been reported to generate ultra-wideband (UWB) signals in the optical domain, but the availability of these methods always relies on small signal modulation. In this paper, the influence of large signal modulation on two typical schemes, representing two major categories of external-modulator-based photonic UWB generation schemes, is analytically and numerically studied. While the quasi single-sideband UWB (QSSB-UWB) pulse can maintain its shape, the Gaussian UWB (GUWB) generation scheme suffers serious modulation distortion when the phase modulation index is greater than $\pi/6$. The modulation distortion would have negative impact on the receiver sensitivity when the signal is sent to a correlation receiver.

OCIS codes: (060.4510) Optical communications; (350.4010) Microwaves; (999.9999) ultra-wideband.

References and links

1. G. R. Aiello and G. D. Rogerson, "Ultra-wideband wireless system," IEEE Microw. Mag. **4**(2), 36–47 (2003).
2. J. P. Yao, F. Zeng, and Q. Wang, "Photonic generation of ultrawideband signals," J. Lightwave Technol. **25**(11), 3219–3235 (2007).
3. C. M. Tan, L. C. Ong, M. L. Yee, B. Luo, and P. K. Tang, "Direct transmission of ultra wide band signals using single mode radio-over-fiber system," Proc. 2005 Asia-Pacific Microw. Conf. (APMC 2005) **1–5**, 1315–1317 (2005).
4. S. L. Pan and J. P. Yao, "UWB-over-fiber communications: modulation and transmission," J. Lightwave Technol. **28**(16), 2445–2455 (2010).
5. M. Ran, B. I. Lembrikov, and Y. Ben Ezra, "Ultra-wideband radio-over-optical fiber concepts, technologies and applications," IEEE Photon. J. **2**(1), 36–48 (2010).
6. Y. Le Guennec, A. Pizzinat, S. Meyer, B. Charboonnier, P. Lombard, M. Lourdiane, B. Cabon, C. Algani, A.-L. Billabert, M. Terre, C. Rurnelhard, J.-L. Polleux, H. Jacquinot, S. Bories, and C. Sillans, "Low-cost transparent radio-over-fiber system for in-building distribution of UWB signals," J. Lightwave Technol. **27**(14), 2649–2657 (2009).
7. R. Llorente, T. Alves, M. Morant, M. Beltran, J. Perez, A. Cartaxo, and J. Marti, "Ultra-wideband radio signals distribution in FTTH networks," IEEE Photon. Technol. Lett. **20**(11), 945–947 (2008).
8. S. L. Pan and J. P. Yao, "Performance evaluation of UWB signal transmission over optical fiber," IEEE J. Sel. Areas Comm. **28**(6), 889–900 (2010).
9. M. Abtahi, M. Mirshafiei, S. LaRochelle, and L. A. Rusch, "All-optical 500-Mb/s UWB transceiver: an experimental demonstration," J. Lightwave Technol. **26**(15), 2795–2802 (2008).
10. X. B. Yu, T. Braidwood Gibbon, M. Pawlik, S. Blaaberg, and I. Tafur Monroy, "A photonic ultra-wideband pulse generator based on relaxation oscillations of a semiconductor laser," Opt. Express **17**(12), 9680–9687 (2009).
11. S. L. Pan and J. P. Yao, "An optical UWB pulse generator for flexible modulation format," IEEE Photon. Technol. Lett. **21**(19), 1381–1383 (2009).
12. J. J. Dong, X. L. Zhang, J. Xu, D. X. Huang, S. N. Fu, and P. Shum, "Ultrawideband monocycle generation using cross-phase modulation in a semiconductor optical amplifier," Opt. Lett. **32**(10), 1223–1225 (2007).
13. S. L. Pan and J. P. Yao, "Switchable UWB pulse generation using a phase modulator and a reconfigurable asymmetric Mach-Zehnder interferometer," Opt. Lett. **34**(2), 160–162 (2009).
14. S. G. Wang, H. W. Chen, M. Xin, M. H. Chen, and S. Z. Xie, "Optical ultra-wide-band pulse bipolar and shape modulation based on a symmetric PM-IM conversion architecture," Opt. Lett. **34**(20), 3092–3094 (2009).

#145774 - $15.00 USD Received 11 Apr 2011; revised 27 May 2011; accepted 19 Jun 2011; published 30 Jun 2011

15. X. H. Feng, Z. H. Li, B. O. Guan, C. Lu, H. Y. Tam, and P. K. A. Wai, "Switchable UWB pulse generation using a polarization maintaining fiber Bragg grating as frequency discriminator," Opt. Express **18**(4), 3643–3648 (2010).
16. Q. Wang and J. P. Yao, "Switchable optical UWB monocycle and doublet generation using a reconfigurable photonic microwave delay-line filter," Opt. Express **15**(22), 14667–14672 (2007).
17. H. Chen, M. Chen, C. Qiu, J. Zhang, and S. Xie, "UWB monocycle pulse generation by optical polarization time delay method," Electron. Lett. **43**(9), 542–543 (2007).
18. J. Li, B. P. P. Kuo, and K. K. Y. Wong, "Ultra-wideband pulse generation based on cross-gain modulation in fiber optical parametric amplifier," IEEE Photon. Technol. Lett. **21**(4), 212–214 (2009).
19. M. Bolea, J. Mora, B. Ortega, and J. Capmany, "Optical UWB pulse generator using an N tap microwave photonic filter and phase inversion adaptable to different pulse modulation formats," Opt. Express **17**(7), 5023–5032 (2009).

1. Introduction

Ultra-wideband (UWB) is a promising technology to provide high data-rate, low cost and low power consumption connectivity for wireless personal area network [1,2]. Due to the low power spectral density specified by the U.S. Federal Communications Commission (FCC), the typical transmission distance of a UWB system is only a few meters to tens of meters. UWB over fiber system is then proposed to increase the coverage area of the UWB system and to integrate the UWB system to other existing wireless and wired networks [2–8].

For UWB over fiber systems, the primary task is to generate optical UWB signals. Until now, a lot of methods have been reported [2, 3, 8–19]. Among them, the methods based on electro-optic modulation are promising for practical UWB over fiber system since electro-optic modulators are simple, reliable and cost effective, which have been widely deployed in the commercial optical communication networks. According to the optical spectral properties of the generated UWB pulses, there are generally three types of UWB generation schemes based on electro-optic modulators [8]: 1) double-side band UWB (DSB-UWB) generation schemes, e.g. converting an electrical UWB pulse to the optical domain based on intensity modulation [3]; 2) quasi single-sideband UWB (QSSB-UWB) generation schemes, e.g. sending an electrical Gaussian pulse to a dual-drive Mach-Zehnder modulator (MZM) with the two paths delayed by tens of picoseconds [11], or phase modulation (PM) by an electrical pulse followed by a detuned optical bandpass filter [12–15]; 3) Gaussian UWB (GUWB) generation schemes, e.g. shaping an electrical pulse by a photonic microwave filter with one negative tap [16–19], or phase modulation (PM) by an electrical pulse followed by a dispersive element [2]. In the three categories, the UWB generation schemes in the second and third categories generates UWB pulses in the time domain, which lead to the advantages such as small size, light weight, and immunity to electromagnetic interference. Although the generation of QSSB-UWB and GUWB signal has been extensively reported in the literature, most of them applied small signal modulation assumption. The small signal modulation can eliminate the nonlinear distortion introduced by electro-optic modulation, but it results in large optical to electrical conversion loss and low signal-to-noise ratio (SNR).

In this paper, we theoretically study the influence of large signal modulation on two typical external-modulator-based schemes for photonic generation of QSSB-UWB and GUWB signals, respectively. The study is aimed to provide the theoretical basis to construct an optical UWB transmitter with small optical to electrical conversion loss and small noise figure for UWB over fiber applications. Since a Gaussian monocycle is the simplest pulse shape among the many suggested UWB waveforms [2], our study is performed based on Gaussian monocycle pulses. The results can be extended to other UWB waveforms, such as Gaussian doublet, Gaussian triplet, and other more complicated waveforms.

2. Analytical analysis

Figure 1 shows the typical schemes to generate the optical QSSB-UWB and GUWB monocycles, respectively. Both of the two schemes are based on an electro-optic modulator. To evaluate the modulation distortion in the electro-optic modulators and their influence on the generated UWB monocycles, the generated optical UWB pulses are introduced to a

#145774 - $15.00 USD Received 11 Apr 2011; revised 27 May 2011; accepted 19 Jun 2011; published 30 Jun 2011

photodetector (PD). All the devices in the schemes are assumed to have flat frequency response in the frequency range of interest.

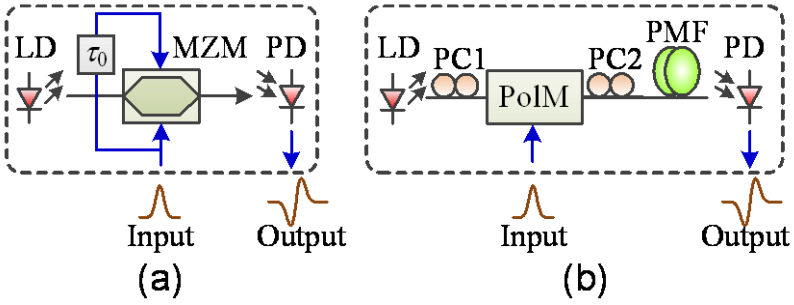

Fig. 1. Configurations of the two typical techniques for the generation of optical UWB monocycles. (a) Generation of QSSB-UWB monocycle using a dual-drive MZM; (b) Generation of GUWB monocycle using a photonic microwave delay-line filter. LD: laser diode, MZM: Mach-Zehnder modulator, PD: photodetector, PC: polarization controller, PolM: polarization modulator, PMF: polarization maintaining fiber.

A. QSSB-UWB

Figure 1(a) shows the scheme for the generation of QSSB-UWB monocycle. In the scheme, an electrical Gaussian pulse train is split into two portions, delayed by a fixed time delay τ_0, and then modulates a light wave from a laser diode (LD) at a dual-drive MZM. The output of the MZM is introduced to a PD for square-law detection, the AC term of the photocurrent can be expressed as [8]

$$I_{\mathrm{AC1}}(t) \propto \mp 2\sin\{\frac{\kappa}{2}[u(t)-u(t-\tau_0)]\} \tag{1}$$

where κ is the phase modulation index, and $u(t)$ represents a Gaussian pulse, given by

$$u(t) = \exp(-\frac{t^2}{2T_0^2}) \tag{2}$$

where T_0 is the half-width (at 1/*e*-intensity point) of the Gaussian pulse. Further expanding (1) based on Taylor expansion, we obtain

$$\begin{aligned} I_{\mathrm{AC1}}(t) \propto & \mp\kappa[u(t)-u(t-\tau_0)] \pm \frac{\kappa^3}{24}[u(t)-u(t-\tau_0)]^3 \mp \frac{\kappa^5}{1920}[u(t)-u(t-\tau_0)]^5 \\ & \pm \frac{\kappa^7}{322560}[u(t)-u(t-\tau_0)]^7 \mp \cdots \end{aligned} \tag{3}$$

To simplify the analysis, we assume $\kappa \leq 2\pi/3$, so the seventh and higher order terms can be ignored since they are less than 1/10 of the fifth-order term. If τ_0 is sufficiently small, $u(t)$-$u(t$-$\tau_0)$ can be approximated as $aw(t)$, where $a<1$, and $w(t)$ is an ideal Gaussian monocycle, given by

$$w(t) = -\frac{t\exp(1/2)}{T_0}\exp\left(-\frac{t^2}{2T_0^2}\right) \tag{4}$$

In order to evaluate the influence of large signal modulation on the receiver sensitivity, a correlation receiver is inserted. In the receiver, the AC term of the photocurrent from the PD is correlated with the ideal Gaussian monocycle. The correlation operation results in

#145774 - $15.00 USD Received 11 Apr 2011; revised 27 May 2011; accepted 19 Jun 2011; published 30 Jun 2011

$$F_1(\tau) \propto \int_{-\infty}^{\infty} I_{AC1}(t) w(t-\tau) dt$$
$$= \int_{-\infty}^{\infty} \{\mp\kappa[u(t)-u(t-\tau_0)] \pm \frac{\kappa^3}{24}[u(t)-u(t-\tau_0)]^3 \mp \frac{\kappa^5}{1920}[u(t)-u(t-\tau_0)]^5\} w(t-\tau) dt \quad (5)$$

As a comparison, the correlation between two ideal monocycles is also presented,

$$F_{ideal}(\tau) = \int_{-\infty}^{\infty} w(t) w(t-\tau) dt \quad (6)$$

From (5) and (6), we can see that the distortion mainly comes from the third- and fifth-order term of (3).

B. GUWB

The GUWB generation scheme shown in Fig. 1(b) consists of a LD, a polarization modulator (PolM), two polarization controllers (PCs) and a section of polarization maintaining fiber (PMF). The PolM driven by an electrical Gaussian pulse generates two complementary intensity-modulated signals along the two orthogonal polarization directions and the PMF introduces a time delay of tens of picoseconds between the two signals. With the square-law detection of a PD, the AC term of the output photocurrent can be expressed as [8]

$$I_{AC2}(t) \propto \mp\{\sin[\kappa u(t)] - \sin[\kappa u(t-\tau_0)]\} \quad (7)$$

Expanding (7) based on Tayor expansion and ignoring the seventh and higher order terms if $\kappa \leq 2\pi/3$, we get

$$I_{AC2}(t) \propto \mp\kappa[u(t)-u(t-\tau_0)] \pm \frac{1}{6}\kappa^3[u^3(t)-u^3(t-\tau_0)] \mp \frac{1}{120}\kappa^5[u^5(t)-u^5(t-\tau_0)] \quad (8)$$

When $I_{AC2}(t)$ is correlated with the ideal monocycle $w(t)$, we have

$$F_2(\tau) \propto \int_{-\infty}^{\infty} I_{AC2}(t) w(t-\tau) dt$$
$$= \int_{-\infty}^{\infty} \{\mp\kappa[u(t)-u(t-\tau_0)] \pm \frac{1}{6}\kappa^3[u^3(t)-u^3(t-\tau_0)] \mp \frac{1}{120}\kappa^5[u^5(t)-u^5(t-\tau_0)]\} w(t-\tau) dt \quad (9)$$

Again, the distortion of correlation mainly comes from the third-and fifth-order of (8). When $\kappa << \pi/6$, the modulation distortion is very small, but when κ is greater than $\pi/6$, the modulation distortion is significant, and should be considered in practical implementation..

With the same phase modulation index κ, the linear terms of (3) and (8) are the same, indicating that the modulation efficiencies for the two schemes are the same. But the third-and fifth-order terms are different, showing that the nonlinear distortions induced by electro-optic modulation are different. If we look at the third-order terms, i.e. $1/24\kappa^3[u(t)-u(t-\tau_0)]^3$ and $1/6\kappa^3[u^3(t)-u^3(t-\tau_0)]$, and considering that $|[u(t)-u(t-\tau_0)]^3| = |[u^3(t)-u^3(t-\tau_0)] - 3u(t)u(t-\tau_0)[u(t)-u(t-\tau_0)]| < |[u^3(t)-u^3(t-\tau_0)]|$, the modulation distortion in the QSSB-UWB generation scheme is much smaller than that of GUWB generation scheme. This difference can also be observed directly from (1) and (7). For the QSSB-UWB generation scheme, the differentiation operation is performed on the amplitude of the optical field. Since $u'(t)\tau_0 \approx u(t)-u(t-\tau_0)$ and τ_0 is very small, $\kappa/2[u(t)-u(t-\tau_0)]$ would also be very small even when κ is as large as π. Thus, the case when κ is large can still be treated as the small signal modulation condition. However, for the GUWB generation scheme, when modulation index is larger than $\pi/6$, $\sin[\kappa u(t)]$ and $\sin[\kappa u(t-\tau_0)]$ cannot be seen as Gaussian pulses, so the subtraction of them is not a Gaussian monocycle pulse. Significant distortion is thus generated.

3. Numerical simulations

To validate the results obtained from the analytical analysis, numerical simulations are performed. The key parameters T_0=39 ps and τ_0=20 ps are selected based on our recent works [11,16].

#145774 - $15.00 USD Received 11 Apr 2011; revised 27 May 2011; accepted 19 Jun 2011; published 30 Jun 2011

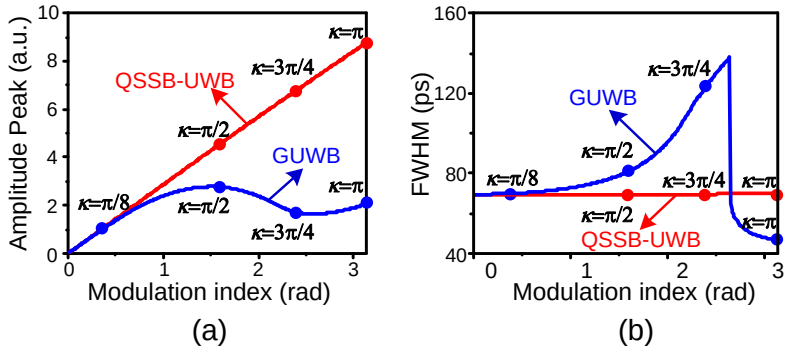

Fig. 2. The (a) amplitude peak and (b) FWHM of the correlations between the ideal UWB monocycle and the QSSB-UWB and GUWB monocycles.

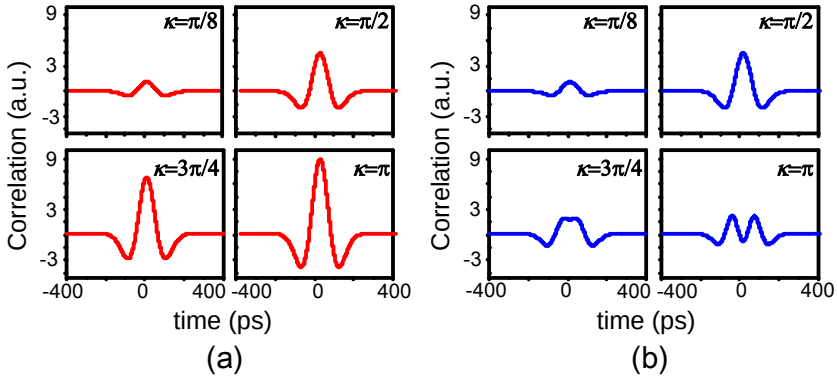

Fig. 3. The curves of correlations between the ideal UWB monocycle and the (a) QSSB-UWB monocycle or (b) GUWB monocycle at four different phase modulation indices.

Figure 2 (a) shows the calculated amplitude peakof the correlations between the ideal UWB monocycle and the QSSB-UWB and GUWB monocycles, i.e. the maximal value of $F_1(\tau)$. When the phase modulation index is smaller than π/6, i.e. small signal modulation is applied, the two curves are almost superimposed, which agrees very well with the analytical results since the linear terms of (3) and (8) are the same and the high-order terms are very small. When the phase modulation index is larger than π/6, i.e. large signal modulation is applied, the linearity of the curve for the QSSB-UWB monocycle is kept, indicating that the QSSB-UWB generation scheme is almost free of modulation distortion. On the other hand, the curve for the GUWB monocycle becomes saturated because the third-order term in (8) increases/decreases faster than that in (3). Especially, when the phase modulation index is larger than π/2, the amplitude peak decreases as the phase modulation index increasing, showing that serious modulation distortion is presented. These results are also confirmed by Fig. 2(b), which gives the full width at half maximum (FWHM) of the correlations between the ideal UWB monocycle and the QSSB-UWB and GUWB monocycles. When the phase modulation index is increased from 0 to π, the FWHM keeps almost the same value (about 70 ps) for the QSSB-UWB monocycle. However, for the GUWB monocycle, the FWHM changes from ~70 to ~140 ps, showing again that the modulation distortion is serious when large signal modulation is performed. Figure 3 shows the curves of correlations between the ideal UWB monocycle and the QSSB-UWB monocycle or GUWB monocycle at four phase modulation indices (π/8, π/2, 3π/4 and π). From Fig. 3, we can see that the shapes of the correlation functions at different phase modulation indices are almost the same for the QSSB-UWB monocycle while double peaks are observed for the GUWB monocycle when the phase

#145774 - $15.00 USD Received 11 Apr 2011; revised 27 May 2011; accepted 19 Jun 2011; published 30 Jun 2011

modulation index is 3π/4 or π. The presence of double peaks can be used to explain the drop of FWHM at the phase modulation index of 2.65 in Fig. 2(b).

In a practical UWB communication system, the signals after correlation are filtered by a low pass filter (LPF) before sent to a decision gate. The receiver sensitivity, which is the minimum value of average received power required to produce a specified signal-to-noise ratio, would be highly related to the signal power obtained after low pass filtering. In general, the decision of 1-bit or 0-bit at the decision gate is made at the center of the pulses, which corresponds to the amplitude peak of the correlation signal, to minimize the possibility of bit errors. Therefore, to evaluate the influence of the large signal modulation on the receiver sensitivity, the amplitude peak of the correlation signal after a LPF is calculated. Three LPFs with different cut-off frequencies (384 MHz, 819.2 MHz and 2 GHz) are considered for three different data rates (480Mb/s, 1024Mb/s and 2.5Gb/s), respectively. Figure 4 shows the calculated amplitude peak against phase modulation index. Since the correlation signal has a lot of high frequency components, larger output power is obtained when LPF with higher cut-off frequency is used. For all the three LPFs, the curves for QSSB-UWB are almost linear. The receiver sensitivity is increased linearly if a large phase modulation index is applied. However, for GUWB, the increase of the electrical power to the modulator would introduce significant modulation distortion, which has negative contribution to the receiver sensitivity, as shown in Fig. 4.

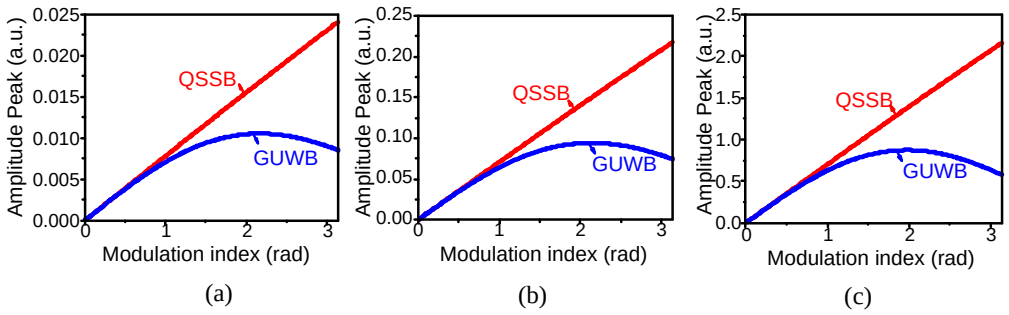

Fig. 4. The calculated amplitude peak of the correlation signal with low pass filtering against phase modulation index. The cut-off frequencies of the low pass filters are (a) 384 MHz, (b) 819.2 MHz and (c) 2 GHz.

4. Conclusion

The influence of large signal modulation on two typical external-modulator-based photonic UWB generation schemes was analytically and numerically studied. Because the differentiation operation is performed on the amplitude of the optical field for the QSSB-UWB generation scheme, and is performed on the optical power for the GUWB generation scheme, QSSB-UWB generation scheme has superior performance over the GUWB generation scheme when large signal modulation is performed, which results in higher receiver sensitivity in a practical UWB communication system. The study suggests an important way to construct a UWB over fiber system with small optical to electrical conversion loss and small noise figure.

Acknowledgements

This work was supported in part by the national Natural Science Foundation of China (NSFC) under grant of 60877043 and 61090392, and the Program for New Century Excellent Talents in University (NCET).

#145774 - $15.00 USD Received 11 Apr 2011; revised 27 May 2011; accepted 19 Jun 2011; published 30 Jun 2011